Diagnostic and Interventional Imaging 000 (2023) 1–8

Original article

Comparison of two deep-learning image reconstruction algorithms on cardiac CT images: A phantom study

Joël Greffier[a,*], Maxime Pastor[a], Salim Si-Mohamed[b,c], Cynthia Goutain-Majorel[d], Aude Peudon-Balas[d], Mourad Zoubir Bensalah[d], Julien Frandon[a], Jean-Paul Beregi[a], Djamel Dabli[a]

[a] *IMAGINE UR UM 103, Montpellier University, Department of Medical Imaging, Nîmes University Hospital, 30029 Nîmes, France*
[b] *University Lyon, INSA-Lyon, University Claude Bernard Lyon 1, UJM-Saint Etienne, CNRS, Inserm, CREATIS UMR 5220, U1206, F–69621, 69100 Villeurbanne, France*
[c] *Department of Radiology, Louis Pradel Hospital, Hospices Civils de Lyon, 69500 Bron, France*
[d] *Department of Medical Imaging, Centre Hospitalier de Perpignan, 66000 Perpignan, France*

ARTICLE INFO

Keywords:
Cardiac CT
Deep-learning image reconstruction algorithm
Multidetector computed tomography
Task-based image quality assessment

ABSTRACT

Purpose: The purpose of this study was to compare the performance of Precise IQ Engine (PIQE) and Advanced intelligent Clear-IQ Engine (AiCE) algorithms on image-quality according to the dose level in a cardiac computed tomography (CT) protocol.
Materials and methods: Acquisitions were performed using the CT ACR 464 phantom at three dose levels (volume CT dose indexes: 7.1/5.2/3.1 mGy) using a prospective cardiac CT protocol. Raw data were reconstructed using the three levels of AiCE and PIQE (Mild, Standard and Strong). The noise power spectrum (NPS) and task-based transfer function (TTF) for bone and acrylic inserts were computed. The detectability index (d') was computed to model the detectability of the coronary lumen (350 Hounsfield units and 4-mm diameter) and non-calcified plaque (40 Hounsfield units and 2-mm diameter).
Results: Noise magnitude values were lower with PIQE than with AiCE (−13.4 ± 6.0 [standard deviation (SD)] % for Mild, -20.4 ± 4.0 [SD] % for Standard and -32.6 ± 2.6 [SD] % for Strong levels). The average NPS spatial frequencies shifted towards higher frequencies with PIQE than with AiCE (21.9 ± 3.5 [SD] % for Mild, 20.1 ± 3.0 [SD] % for Standard and 12.5 ± 3.5 [SD] % for Strong levels). The TTF values at fifty percent (f_{50}) values shifted towards higher frequencies with PIQE than with AiCE for acrylic inserts but, for bone inserts, f_{50} values were found to be close. Whatever the dose and DLR level, d' values of both simulated cardiac lesions were higher with PIQE than with AiCE. For the simulated coronary lumen, d' values were better by 35.1 ± 9.3 (SD) % on average for all dose levels for Mild, 43.2 ± 5.0 (SD) % for Standard, and 62.6 ± 1.2 (SD) % for Strong levels.
Conclusion: Compared to AiCE, PIQE reduced noise, improved spatial resolution, noise texture and detectability of simulated cardiac lesions. PIQE seems to have a greater potential for dose reduction in cardiac CT acquisition.

1. Introduction

In recent years, with the emergence of artificial intelligence in medicine, algorithms for the reconstruction of computed tomography (CT) images based on deep learning (DLR) have been developed [1]. These algorithms feature a deep neural network (DNN) [2,3] or a convolutional neural network (CNN) [4–6] to differentiate the signal from the noise and thus reduce the noise in the image without altering its texture. These new algorithms are used in clinical routine and can provide better image quality for the same dose level or even a lower dose, whilst maintaining a diagnostic image quality similar to that of iterative reconstruction algorithms [2,3,5-17].

A new DLR algorithm (Advanced intelligent Clear-IQ Engine [AiCE]) that features a DNN trained with high-quality model-based iterative reconstruction patient datasets has been recently developed [7,18]. A second version of this algorithm was later developed. Since the first version, new reconstruction kernels and slice thicknesses have become available [7]. In addition, its DNN has been trained with a larger patient database, resulting in reduced noise and better spatial resolution and detectability without changing the noise texture [7].

Abbreviations: AICE, Advanced intelligent Clear-IQ Engine; CNN, Convolutional neural network; CT, Computed tomography; $CTDI_{vol}$, Volume CT dose index; DLR, Deep-learning image reconstruction; DNN, Deep neural network; HU, Hounsfield unit; NPS, Noise power spectrum; PIQE, Precise IQ Engine; SD, Standard deviation; SR-DLR, Super-resolution deep-learning image reconstruction; TTF, Task-based transfer function

* Corresponding author.
E-mail address: joel.greffier@chu-nimes.fr (J. Greffier).

https://doi.org/10.1016/j.diii.2023.10.004
2211-5684/

In cardiac imaging, high-resolution imaging is of great interest for detecting lesions such as calcified or non-calcified coronary plaques [19–22]. Such imaging protocols require acquisitions with low nominal slice thicknesses thus increasing image noise, which can be tackled either by an increase in the X-ray dose or with image reconstruction. AiCE, reduces noise, which is especially abundant in low radiation dose images, improves signal-to-noise ratio, and maintains noise texture, which is a limitation of iterative reconstruction [1]. The Precise IQ Engine (PIQE) is a new specially trained super-resolution DLR (SR-DLR) algorithm, dedicated to cardiac image reconstruction. The neural network of PIQE features a three-dimensional deep CNN trained using cardiac image data acquired on the commercially available ultra-high resolution CT scanner (Aquilion Precision), which in clinical practice uses 0.25 mm detector elements. The raw data coming from this CT system and used to train the neural network are reconstructed with AiCE. This new SR-DLR algorithm is currently available only for cardiac cases, on the wide-area detector Aquilion ONE / PRISM Edition CT system [23]. On this CT system, PIQE can be used with two reconstructed image thicknesses of 0.5 and 1 mm combining volume acquisitions.

Recent attempts of high-resolution imaging with spiral CT are encountering difficulties such as radiation exposure and scan heart rate variability [24,25]. Several studies have highlighted AiCE's contribution to improving the quality of cardiac CT images compared to the iterative reconstruction algorithm Adaptive Iterative Dose Reduction (AIDR 3D) [10,16,26]. These studies showed that, compared to AIDR 3D, at the same dose level, AiCE improves the image quality of coronary CT angiography images and reduces the image noise [10,16,26]. Another study has shown that AiCE improves the quality of coronary CT angiography images with a dose reduction of about 40 % compared to AIDR 3D [14]. One clinical study showing the superiority of PIQE over an iterative algorithm for coronary CT angiography has been published [27]. Two phantom studies have also compared PIQE with AiCE and two other iterative reconstruction algorithms using task-based image quality assessment [28,29]. In the first study, acquisition and reconstruction parameters different from those used for routine clinical cardiac CT were used [29]. In addition, the detectability index was calculated on the iodine insert and not on simulated lesions with clinical features. In the second study, only one of the 3 levels (the level Standard) available for AiCE and PIQE were assessed [28].

The purpose of this study was to assess the impact of the new SR-DLR algorithm, PIQE on the quality of cardiac CT images compared with the DLR algorithm AiCE using all the levels available for these two algorithms and dose levels used in clinical routine.

2. Materials and methods

2.1. Acquisitions and reconstruction parameters

An anthropomorphic phantom (CT Torso CTU-41; Kyoto Kagaku) and a 20 cm diameter image quality phantom (CT ACR 464; Sun Nuclear) phantom were scanned on an Aquilion ONE / PRISM Edition CT system (Canon Medical Systems Corporation, Otawara, Japan) equipped with the AiCE DLR algorithm and the new cardiac SR-DLR algorithm, PIQE.

Acquisitions were performed on a single-rotation cardiac coverage of 16 cm in axial mode (physical beam collimation of 320 × 0.5 mm^2) using the prospective CT cardiac protocol. For each acquisition, a heart rate of 60 beats/min was simulated and the acquisition was performed on a single cardiac cycle (75 % of the RR interval). Classical acquisition cardiac CT parameters were used including a tube voltage of 100 kVp, a rotation time of 0.275 s/rotation and a field-of-view of 220.7 mm. The tube current modulation system was disabled and the tube current (mA) was set to obtain CT volume dose indexes ($CTDI_{vol}$) close to 7.1, 5.2 and 3.1 mGy (900, 650 and 400 mA, respectively). The first dose level corresponds to the dose level usually used in clinical routine, and the other two levels have been used to assess the impact of dose reduction on image quality with these two DLR algorithms. For each dose level, five acquisitions were performed on the image quality phantom and only one acquisition for the anthropomorphic phantom.

Raw data were reconstructed using the three levels of AiCE and PIQE (Mild/Standard/Strong), the "Cardiac" reconstruction kernel, a matrix of 512 × 512 pixels, a slice thickness close to 0.5 mm (0.25 mm increments) and a 220 mm field-of-view.

2.2. Task-based image quality assessement

A task-based image quality assessment was performed using the iQMetrix-CT software developed by a working group from the French Society of Medical Physicists [30].

2.2.1. Task-based transfer function

The task-based transfer function (TTF) was used to assess the spatial resolution under conditions of contrast and noise, close to the lesions encountered in clinical practice. It was calculated on acrylic and bone inserts of the image quality phantom (Fig. 1.A) using the circular edge technique [31,32]. To minimize the image-noise effect on the edge spread function, the TTF was computed from 200 consecutive axial slices (40 slices for each of the five acquisitions).

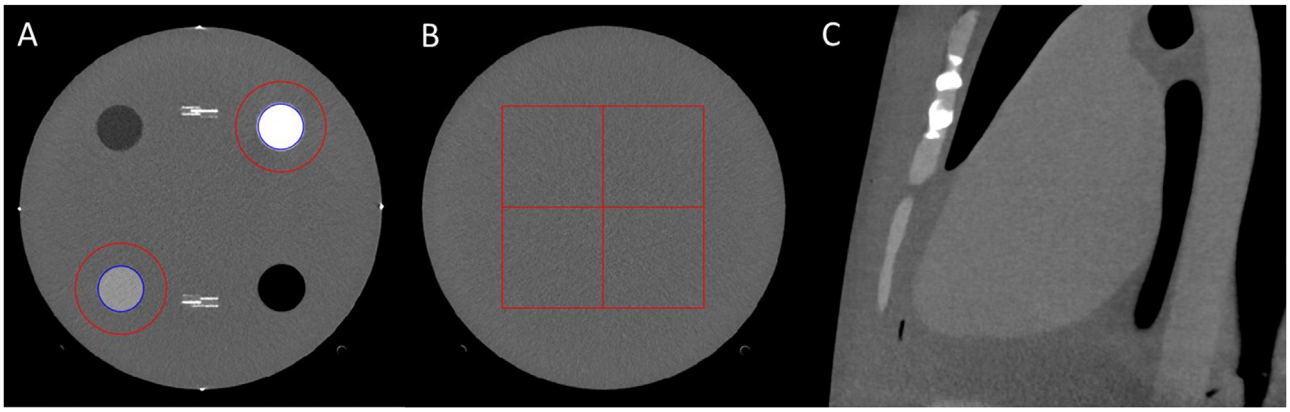

Fig. 1. Photographs of the phantoms used in the study. A: Figure shows region of interest (ROIs) in red used to compute the task-based transfer function (TTF) with the acrylic and bone inserts. B: Figure shows ROIs in red used for the noise power spectrum (NPS) assessment. C: Figure shows sagittal view of the heart of the anthropomorphic phantom.

2.2.2. Noise power spectrum

The noise power spectrum (NPS) is used to evaluate noise texture and noise magnitude in the frequency domain. It was computed on the same number of slices as defined for the TTF by placing four square regions of interest (ROIs) of 128 × 128 pixels in the homogeneous module of the image quality phantom (Fig. 1.B) as follows (1):

$$NPS_{2D}(f_x,f_y) = \frac{\Delta_x\Delta_y}{L_xL_y}\frac{1}{N_{ROI}}\sum_{i=1}^{N_{ROI}}|FFT_{2D}\{ROI_i(x,y) - FIT_i(x,y)\}|^2 \quad (1)$$

where Δ_x and Δ_y are the pixel size in the x- and y-directions, respectively; *FFT* is the fast Fourier transform; L_x and L_y are the lengths of the ROIs in the x- and y-directions; N_{ROI} is the number of ROIs; $ROI_i(x,y)$ is the mean pixel value measured for a ROI in its position (x,y) and $FIT_i(x,y)$ is a 2nd order polynomial fit of $ROI_i(x,y)$.

To quantify the changes in noise magnitude and noise texture of the image, the square root of the area under the NPS curve and the weighted average spatial frequency (f_{av}, mm^{-1}) of the NPS1D curve were measured [32].

2.2.3. Detectability index

A non-prewhitening observer model with an eye filter (NPWE) was used to calculate the detectability index (d'_{NPWE}):

$$d'^2_{NPWE} = \frac{\left[\iint |W(u,v)|^2.TTF(u,v)^2.E(u,v)^2 dudv\right]^2}{\iint |W(u,v)|^2.TTF(u,v)^2.NPS(u,v).E(u,v)^4 dudv} \quad (2)$$

where *u* and *v* are the spatial frequencies in the x- and y-directions, *E* the eye filter that models the human visual system sensitivity to different spatial frequencies [33–35], and *W(u,v)* the task function defined as:

$$W = |F\{h_1(x,y) - h_2(x,y)\}| \quad (3)$$

where F is the Fourier transform and $h_1(x,y)$ and $h_2(x,y)$ correspond to the object present and the object absent hypotheses, respectively [32].

The eye filter was modeled according to the human visual response function [35] using a zoom factor of 1.5 and a 500 mm viewing distance.

Two task functions were defined: one with a diameter of 2 mm and a contrast of 40 Hounsfield units (HU) to simulate the non-calcified plaque and the second with a diameter of 4 mm and a contrast of 350 HU to simulate the coronary lumen [22]. TTF results from the acrylic insert were used for the detection task of the non-calcified plaque whereas the results of the bone insert were used for the coronary lumen.

2.3. Subjective image quality assessment

Axial cardiac images of the anthropomorphic phantom obtained for both the DLR and SR-DLR algorithms and all dose levels were scored in consensus by two radiologists (S. S.-M. and M.P., with 13 and six years of experience, respectively) using the previously published methodology (Fig. 1.C) [2,8]. Readers were blinded to the dose level and reconstruction type (algorithm and levels). They were instructed to subjectively assess image noise, image smoothing, image sharpness and the contrast between vessels and fat in the mediastinum using a commonly used five-point scale in which 1 = unacceptable, 2 = suboptimal, 3 = acceptable, 4 = above average, and 5 = excellent. The overall image quality was scored using a four-point scale: 1 = not evaluable, 2 = interpretable despite moderate artifacts or noise, 3 = fully interpretable with mild artifacts or noise, 4 = no artifacts or noise [2,8]. A value < 3 was considered unsatisfactory for clinical use.

2.4. Statistical analysis

The normality of the distribution of quantitative variables was test using Shapiro-Wilk test [36]. Quantitative variables were expressed as means ± standard deviations (SD) and ranges when normally distributed.

3. Results

3.1. Noise power spectrum

3.1.1. Noise magnitude

For both DLR and SR-DLR algorithms, noise magnitude decreased as the dose level increased and from the Mild level to Strong level (Table 1 and Fig. 2). For AiCE, noise magnitude decreased for all dose levels by −9.8 % ± 1.2 (SD) % from Mild to Standard and −10.5 % ± 1.5 (SD) % from Standard to Strong on average. For PIQE, noise magnitude decreased by −16.6 % ± 9.4 (SD) % and −24.2 % ± 4.3 (SD) % on average, respectively.

For all dose levels and each DLR level, noise magnitude values were lower with PIQE than with AiCE. The noise magnitude differences between PIQE and AiCE increased as the DLR level increased (on average by −13.4 ± 6.0 [SD] % for Mild, −20.4 ± 4.0 [SD] % for Standard and −32.6 ± 2.6 [SD] % for Strong).

3.1.2. Noise texture

For each algorithm and each DLR level, similar f_{av} values were found according to dose level (Table 1 and Fig. 2). For AiCE, f_{av} values shifted towards lower frequencies from Mild (0.31 ± 0.01 [SD] mm^{-1}) to Strong (0.27 ± 0.01 [SD] mm^{-1}) levels. The same pattern was found for PIQE: 0.37 ± 0.01 [SD] mm^{-1} and 0.31 ± 0.02 [SD] mm^{-1}, respectively.

For all dose levels and each DLR level, f_{av} values were greater with PIQE than with AiCE. The differences in f_{av} values between PIQE and AiCE decreased as the DLR level increased (by 21.9 ± 3.5 [SD] % for Mild, 20.1 ± 3.0 [SD] % for Standard and 12.5 ± 3.5 [SD] % for Strong, on average).

Table 1
Noise magnitude and average noise power spectrum (NPS) spatial frequencies (f_{av}) obtained for all dose levels and the three levels of AiCE and PIQE algorithms.

Variable	$CTDI_{vol}$ (mGy	AiCE			PIQE		
		Mild	Standard	Strong	Mild	Standard	Strong
Noise magnitude (HU)	3.1	19.3	17.2	15.1	17.9	13.0	9.8
	5.2	16.8	15.1	13.5	14.3	12.7	9.1
	7.1	15.2	13.9	12.6	12.3	11.0	8.8
f_{av} (mm^{-1})	3.1	0.30	0.28	0.27	0.38	0.33	0.29
	5.2	0.31	0.29	0.28	0.37	0.36	0.31
	7.1	0.31	0.30	0.28	0.37	0.36	0.32

AiCE: Advanced intelligent Clear-IQ Engine; $CTDI_{vol}$: volume CT dose index; PIQE: Precise IQ Engine.

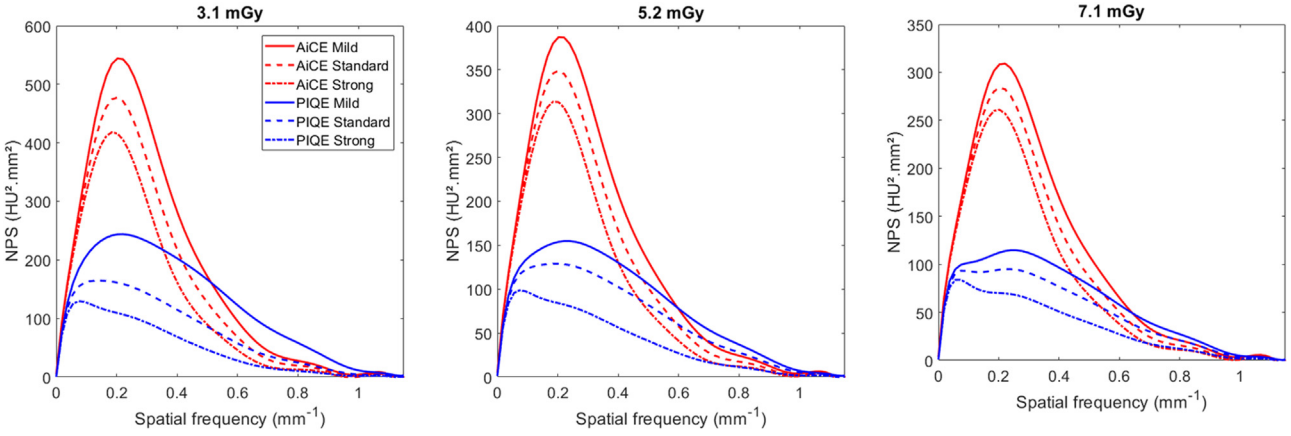

Fig. 2. Graph show noise power spectrum (NPS) curves obtained for all levels of AiCE and PIQE and the three dose levels.
Noted that the iQMetrix-CT software only guarantees NPS data calculated up to Nyquist frequency.

3.2. Task-based transfer function

For both inserts, TTF curves are depicted in Fig. 3 and values for TTF at fifty percent (f_{50}) are shown in Table 2.

For the acrylic insert and for each DLR algorithm (Fig. 3.A), similar f_{50} values were found for all dose and DLR levels (0.30 ± 0.02 [SD] mm^{-1} for AiCE and 0.40 ± 0.01 [SD] mm^{-1} for PIQE). For each DLR level, f_{50} values shifted toward higher frequencies with PIQE compared to AiCE (on average by 31.0 ± 4.1 [SD] % for Mild, 32.5 ± 1.3 [SD] % for Standard and 33.7 ± 2.7 [SD] % for Strong levels).

For the bone insert and both algorithms (Fig. 3.B), f_{50} values decreased as the dose increased, especially from 3.1 to 5.2 mGy. For AiCE, f_{50} values increased from Mild to Standard (4.9 ± 1.0 [SD] %) and from Standard to Strong (4.3 ± 0.9 [SD] %) levels. For PIQE and each dose level, similar f_{50} values were found for all DLR levels (0.5 ± 2.0 [SD] % from Mild to Standard and −0.8 ± 1.0 [SD] % from Standard to Strong). f_{50} values shifted toward higher frequencies with PIQE than with AiCE for Mild (8.3 ± 1.5 [SD] %) and Standard (3.7 ± 1.5 [SD] %) levels. For Strong level, similar f_{50} values were found with AiCE and PIQE algorithms (−1.3 ± 0.1 [SD] %).

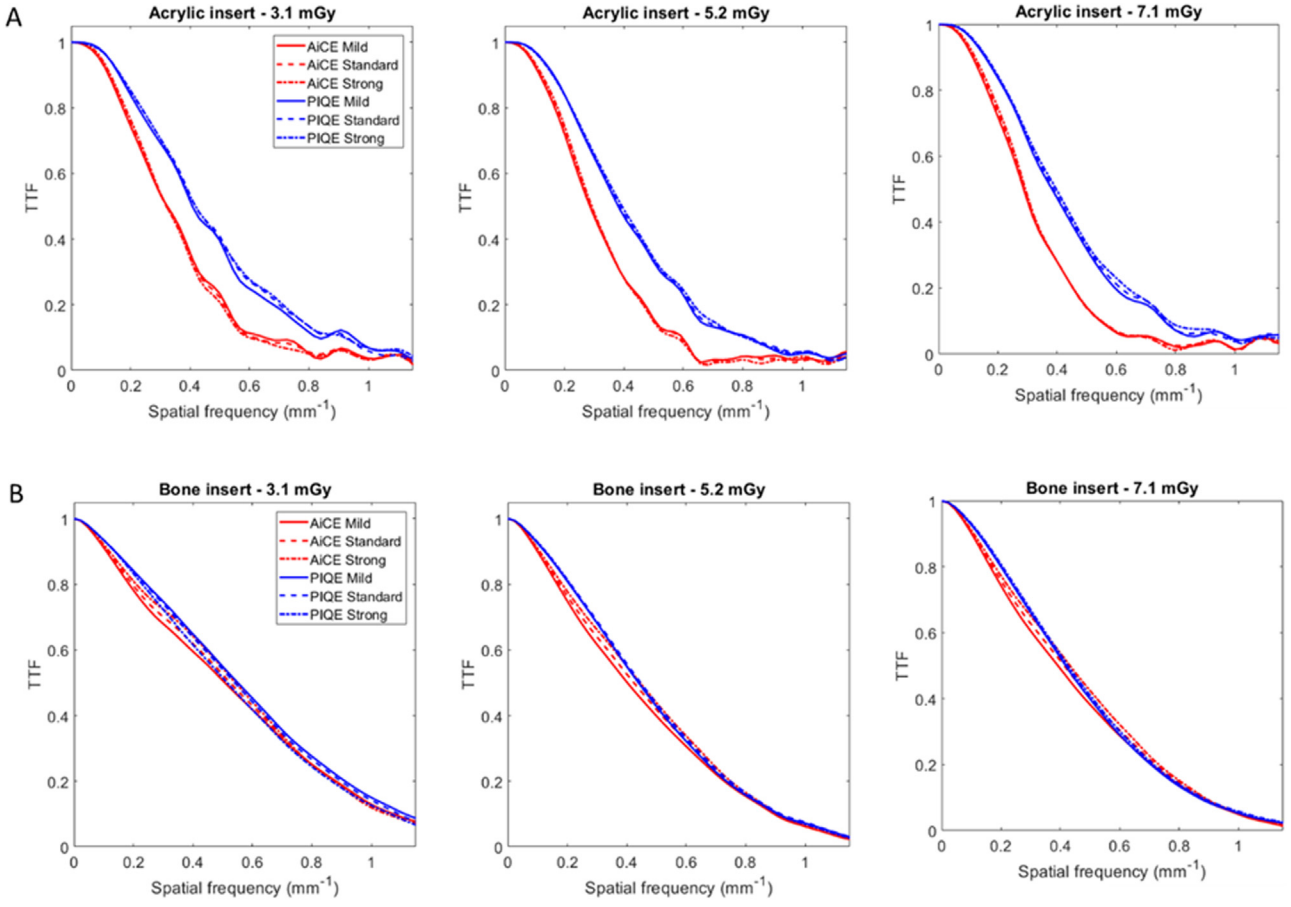

Fig. 3. Graph show task-based transfer function (TTF) curves obtained for all levels of AiCE and PIQE and the three dose levels for acrylic (A) and bone (B) inserts.
Noted that the iQMetrix-CT software only guarantees TTF data calculated up to Nyquist frequency.

Table 2
Task-based transfer function values at fifty percent (f_{50}) of the acrylic and bone inserts obtained for all dose levels and the three levels of AiCE and PIQE algorithms.

Variable	$CTDI_{vol}$ (mGy)	AiCE			PIQE		
		Mild	Standard	Strong	Mild	Standard	Strong
f_{50} (mm^{-1}) bone insert	3.1	0.51	0.53	0.54	0.55	0.54	0.52
	5.2	0.40	0.42	0.45	0.44	0.45	0.44
	7.1	0.39	0.41	0.43	0.42	0.43	0.43
f_{50} (mm^{-1}) acrylic insert	3.1	0.32	0.32	0.32	0.41	0.42	0.42
	5.2	0.29	0.29	0.29	0.38	0.39	0.39
	7.1	0.29	0.29	0.29	0.38	0.39	0.40

AiCE: Advanced intelligent Clear-IQ Engine; $CTDI_{vol}$: volume CT dose index; PIQE: Precise IQ Engine.

3.3. Detectability index

Fig. 4 depicts the d'_{NPWE} values obtained for all dose levels and both DLR algorithms. For the two simulated cardiac lesions, d'_{NPWE} increased as the dose increased and from Mild to Strong levels. d'_{NPWE} values were higher for coronary lumen (Fig. 4.A) than for non-calcified plaque (Fig. 4.B).

For both simulated lesions, d'_{NPWE} values were higher with PIQE than AiCE for the same DLR level. For the coronary lumen, d' values increased by 35.1 ± 9.3 (SD) % for Mild, 43.2 ± 5.0 (SD) % for Standard and 62.6 ± 1.2 (SD) % for Strong levels on average. For the non-calcified plaque, d'_{NPWE} values increased by 60.3 ± 10.3 (SD) % for Mild, 70.7 ± 5.3 (SD) % for Standard and 93.4 ± 2.5 (SD) % for Strong levels, on average.

3.4. Subjective image quality

Fig. 5 shows the image quality obtained with the anthropomorphic phantom and Table 3 shows the results of subjective image quality assessed by the two radiologists.

For both DLR algorithms, the scores of image noise, image sharpness and contrast between vessels and fat increased as the dose increased and from Mild to Strong levels. For the image smoothing, the score tended to decrease from Mild level at 3.1 mGy to Strong

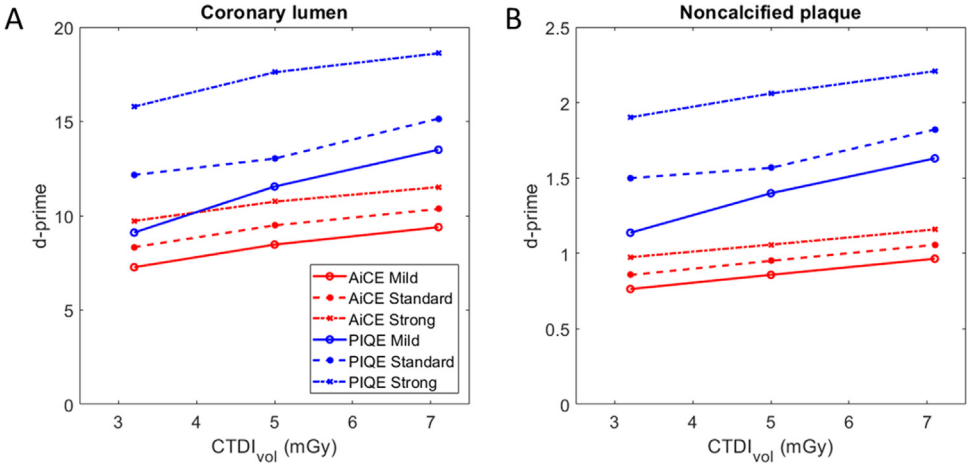

Fig. 4. Graph show detectability index (d') values of the coronary lumen (A. 4 mm in diameter, 350 HU contrast), and non-calcified plaque (B. 2 mm in diameter, 40 HU contrast) obtained for all levels of AiCE and PIQE and the three dose levels.

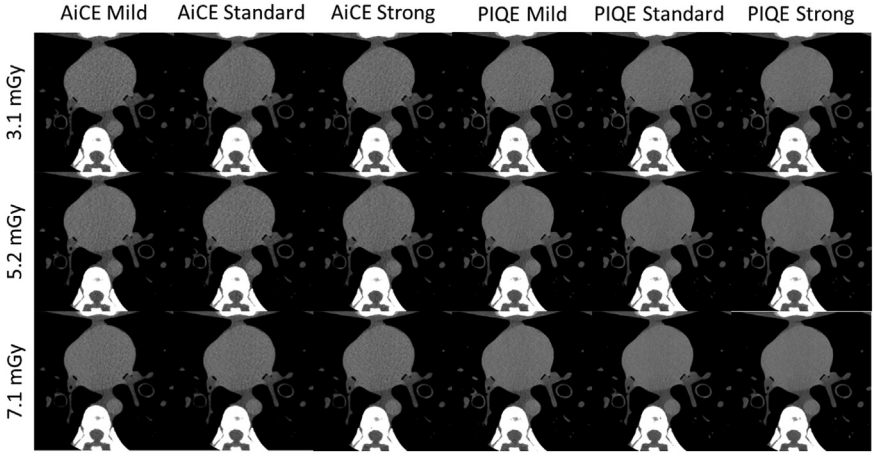

Fig. 5. Figure show axial anthropomorphic CT images (WL: 400 HU, WW: 40 HU) obtained for all levels of AiCE and PIQE and the three dose levels.

Table 3
Results of subjective image quality.

Variable	$CTDI_{vol}$ (mGy)	AiCE			PIQE		
		Mild	STD	STR	Mild	STD	STR
Image noise (scores 1–5)	3.1	**2.5**	3.0	3.5	3.5	4.0	4.5
	5.2	3.0	3.5	4.0	4.0	4.5	4.5
	7.1	4.0	4.5	5.0	4.5	4.5	5.0
Image smoothing (scores 1–5)	3.1	3.5	3.5	3.0	3.5	3.5	3.0
	5.2	3.5	3.5	3.5	4.0	4.0	3.5
	7.1	4.0	3.5	3.5	4.5	4.0	4.0
Image sharpness (scores 1–5)	3.1	**2.5**	3.5	4.0	3.5	4.0	4.5
	5.2	3.0	3.5	4.0	4.5	4.5	4.5
	7.1	4.0	4.0	4.5	4.5	5.0	5.0
Contrast between vessels and fat in the mediastinum (scores 1–5)	3.1	**2.5**	3.5	3.5	4.0	4.0	4.5
	5.2	3.0	3.5	3.5	4.0	4.5	5.0
	7.1	3.5	4.0	4.5	4.5	5.0	5.0
Overall image quality (scores 1–4)	3.1	**2.0**	**2.5**	3.0	3.0	3.5	3.5
	5.2	**2.5**	3.0	3.0	4.0	3.5	4.0
	7.1	3.0	3.5	4.0	4.0	4.0	4.0

Bold indicates values < 3, which were considered unsatisfactory for clinical use. AiCE: Advanced intelligent Clear-IQ Engine; $CTDI_{vol}$: volume CT dose index; PIQE: Precise IQ Engine.

level at 7.1 mGy. For the same DLR level, the scores for image noise, image sharpness, image smoothing and contrast were higher or similar with PIQE than with AiCE.

For the same dose level and the same DLR level, the overall image quality score were higher or similar with PIQE compared to AiCE. For PIQE, radiologists rated the overall image quality ≥ 3 for all dose levels and all DLR levels. For AiCE, the overall image quality was ≥ 3, except at 3.1 and 5.2 mGy with Mild level and at 3.1 mGy with Standard level.

4. Discussion

In the present study, the new PIQE cardiac SR-DLR algorithm's contribution to improving the quality of cardiac CT images was assessed. To this aim, a task-based image quality assessment and subjective image quality assessment were performed and the results obtained with PIQE were compared with those of the AiCE DLR algorithm used so far. Compared to AiCE, the noise magnitude was reduced and the spatial resolution and the noise texture were improved with PIQE at all dose levels. Radiologists confirmed these results in their subjective image quality assessment of cardiac images of the anthropomorphic phantom. Greater detectability was found with PIQE than with AiCE for the two simulated cardiac lesions.

The NPS outcomes confirmed that for AiCE algorithm, noise magnitude decreased as the dose level increased and from Mild to Standard levels [18,29]. The same pattern was found for PIQE algorithm. For the same dose level and DLR level, noise magnitude was lower with PIQE than with AiCE [28,29]. Regarding the noise texture outcomes, f_{av} values shifted toward lower spatial frequencies from Mild to Strong levels for both algorithms. For each dose and DLR level, f_{av} values were shifted toward higher spatial frequencies with PIQE than with AiCE indicating that the image texture was less changed notably the image smoothing was less important. Similar noise magnitude and noise texture outcomes according to the dose and DLR levels were found in another study [29]. The radiologists confirmed the noise magnitude and noise texture outcomes on the subjective assessment of the cardiac images of the anthropomorphic phantom. The scores for noise magnitude and noise texture were considered satisfactory for clinical use for almost all dose levels and all DLR levels of both algorithms, except for AiCE Mild at 3.1 mGy. The noise reduction and noise texture improvement obtained with PIQE compared to AiCE might be related to the fact that the PIQE's CNN was trained with high resolution images reconstructed with AiCE whereas AiCE's DNN was trained with high quality images reconstructed with the FIRST MBIR algorithm. However, one study showed that compared to FIRST and AIDR 3D algorithms, AiCE had lower noise magnitude values and higher or similar f_{av} values depending on the DLR level [18].

The TTF results showed that for both inserts studied, the f_{50} values representing spatial resolution, varied depending on the insert and algorithm used. For the low contrast acrylic insert, f_{50} values were not influenced by the dose level and the DLR level for either of the two algorithms. Similar outcomes were found with the iodine insert in another image quality phantom [29]. For the high contrast bone insert, the f_{50} values decreased between $CTDI_{vol}$ values of 3.1 to 5.2 mGy for all DLR levels of both algorithms and according to the DLR level only for AiCE. For AiCE, the f_{50} values were lower for the acrylic insert than for the bone insert. For PIQE, the same pattern was observed but with less difference between f_{50} values. With this behavior, the f_{50} values were higher with PIQE than with AiCE for the acrylic insert whereas the values were close for the bone insert. These results might be explained by the non-linear properties (spatial resolution is dependent on noise and contrast) of the FIRST algorithm used to train the AiCE's DNN. One study showed that with a soft tissue kernel, when AiCE was used to train the PIQE's CNN, it also exhibited non-linear properties but the spatial resolution was less impacted than the FIRST algorithm by the contrast of the inserts [18]. In addition, radiologists rated the image sharpness (contours of the aorta and heart) and contrast between the vessels and the mediastinum of the cardiac images with higher scores for PIQE than for AICE. For these two criteria, all images of both algorithms were rated satisfactory for clinical use. The higher spatial resolution values of PIQE compared to AiCE may be related to the fact that AiCE is a versatile DLR designed for various medical imaging modalities, including cardiac CT. It aims to provide high-quality images by reducing noise and enhancing image clarity across different applications. On the other hand, PIQE is specifically dedicated to cardiac imaging, focusing on optimizing the reconstruction process for cardiac CT scans. Also, AiCE is trained using high-quality images reconstructed with the FIRST MBIR algorithm. In contrast, the CNN of PIQE is trained from ultra-high resolution cardiac datasets acquired on a CT system with a 0.25 mm nominal slice thickness and is specifically tailored for cardiac imaging.

The detectability index results confirmed that the d' values increased as the dose level and the lesion contrast increased but also from Mild to Strong AiCE levels [18,29]. For both simulated cardiac lesions and each DLR level, d' values were higher with PIQE than AiCE. These results were directly related with the NPS and TTF outcomes where PIQE had lower image noise, a higher noise texture, and higher or similar spatial resolution compared to AiCE. Similar outcomes were found for the detectability of iodine insert [29] or other inserts [28]. In addition, the d' values obtained for all dose levels and all DLR levels with PIQE were higher than the d' values obtained with the highest level of AiCE (Strong) and the highest dose level (7.1 mGy), except for the level Mild of PIQE. This result opens very interesting perspectives on the potential of PIQE for optimizing the doses delivered to patients in cardiac CT protocols. Subjective phantom-based assessment performed by the radiologists showed that overall image quality was satisfactory for clinical use for all levels of PIQE and all dose levels. Finally, based on the results obtained for the d' values of the two simulated lesions and the results of the subjective analysis on anthropomorphic phantom, PIQE could be used in clinical routine with a Standard or Strong level at any dose level, including the lowest investigated, in this study, 3.1 mGy. This would continue to address the challenge of obtaining high-resolution images for cardiac imaging without increasing the patient radiation dose, which has already been improved by the AICE algorithm. Our outcomes must now be validated in a cohort of patients for routine cardiac CT taking into account the patient's heart rate, morphology and the contrast of the coronary arteries injected with contrast media.

This study has its limitations. The comparison of both DLR algorithms was performed with specific acquisition and reconstruction parameters and other outcomes could have been obtained with other parameters (dose level, slice thickness). This study was conducted on phantoms that did not take into account the patient's body morphology. Both phantoms used were static, which may have led to an overestimation of detectability. Last, in addition to this preliminary phantom study, an evaluation of these two reconstruction algorithms by radiologists should be performed. This could include the evaluation of specific cardiac anomalies and pathologies such as coronary artery stenosis, myocardial infarction, cardiac masses (such as tumors or thrombi), congenital cardiac anomalies, valvular diseases, and aortic pathologies (such as aneurysms or dissections).

In conclusion, AiCE has already demonstrated its ability to enhance image quality and achieve dose reduction in cardiac CT imaging, while the results of this study showed that PIQE will continue to improve the quality of cardiac CT images by reducing noise and improving image texture, spatial resolution and detectability of lesions. Further patient studies must now be conducted to validate and confirm these preliminary findings on phantoms and to assess the clinical impact of both algorithms.

Human rights

Not applicable for phantom studies.

Informed consent and patient details

Not applicable for phantom studies.

Author contributions

All authors attest that they meet the current International Committee of Medical Journal Editors (ICMJE) criteria for Authorship.

Declaration of Competing Interest

The authors have no conflicts of interest to disclose.

CRediT authorship contribution statement

Joël Greffier: Conceptualization, Data curation, Formal analysis, Funding acquisition, Investigation, Methodology, Software, Supervision, Validation, Writing – original draft, Writing – review & editing. **Maxime Pastor:** Visualization, Writing – original draft, Writing – review & editing. **Salim Si-Mohamed:** Visualization, Writing – original draft, Writing – review & editing. **Cynthia Goutain-Majorel:** Funding acquisition, Investigation, Writing – original draft, Writing – review & editing. **Aude Peudon-Balas:** Funding acquisition, Investigation, Writing – original draft, Writing – review & editing. **Jean-Paul Beregi:** Project administration, Resources, Supervision, Writing – original draft, Writing – review & editing. **Djamel Dabli:** Conceptualization, Data curation, Formal analysis, Funding acquisition, Investigation, Methodology, Software, Validation, Writing – original draft, Writing – review & editing.

Funding information

This study received no funding.

Acknowledgements

We thank Teresa Sawyers, Medical Writer at the BESPIM, Nîmes University Hospital, for her help in revising the manuscript. We thank Anthony Thay (Canon Medical France) and Christina Balta (Canon Medical Europe) for their help to perform this study. We would also like to thank the medical imaging department at the Hospital Center of Perpignan for allowing us to perform these measurements on their CT system.

References

[1] Willemink MJ, Noel PB. The evolution of image reconstruction for CT-from filtered back projection to artificial intelligence. Eur Radiol 2019;29:2185–95.
[2] Greffier J, Frandon J, Si-Mohamed S, Dabli D, Hamard A, Belaouni A, et al. Comparison of two deep learning image reconstruction algorithms in chest CT images: a task-based image quality assessment on phantom data. Diagn Interv Imaging 2022;103:21–30.
[3] Greffier J, Hamard A, Pereira F, Barrau C, Pasquier H, Beregi JP, et al. Image quality and dose reduction opportunity of deep learning image reconstruction algorithm for CT: a phantom study. Eur Radiol 2020;30:3951–9.
[4] Gogin N, Viti M, Nicodème L, Ohana M, Talbot H, Gencer U, et al. Automatic coronary artery calcium scoring from unenhanced-ECG-gated CT using deep learning. Diagn Interv Imaging 2021;102:683–90.
[5] Greffier J, Frandon J, Durand Q, Kammoun T, Loisy M, Beregi JP, et al. Contribution of an artificial intelligence deep-learning reconstruction algorithm for dose optimization in lumbar spine CT examination: a phantom study. Diagn Interv Imaging 2023;104:76–83.
[6] Greffier J, Durand Q, Frandon J, Si-Mohamed S, Loisy M, de Oliveira F, et al. Improved image quality and dose reduction in abdominal CT with deep-learning reconstruction algorithm: a phantom study. Eur Radiol 2023;33:699–710.
[7] Greffier J, Dabli D, Frandon J, Hamard A, Belaouni A, Akessoul P, et al. Comparison of two versions of a deep learning image reconstruction algorithm on CT image quality and dose reduction: a phantom study. Med Phys 2021;48:5743–55.
[8] Greffier J, Si-Mohamed S, Frandon J, Loisy M, de Oliveira F, Beregi JP, et al. Impact of an artificial intelligence deep-learning reconstruction algorithm for CT on image quality and potential dose reduction: a phantom study. Med Phys 2022;49:5052–63.
[9] Franck C, Zhang G, Deak P, Zanca F. Preserving image texture while reducing radiation dose with a deep learning image reconstruction algorithm in chest CT: a phantom study. Phys Med 2021;81:86–93.
[10] Tatsugami F, Higaki T, Nakamura Y, Yu Z, Zhou J, Lu Y, et al. Deep learning-based image restoration algorithm for coronary CT angiography. Eur Radiol 2019;29:5322–9.
[11] Lenfant M, Chevallier O, Comby PO, Secco G, Haioun K, Ricolfi F, et al. Deep learning versus iterative reconstruction for CT pulmonary angiography in the emergency setting: improved image quality and reduced radiation dose. Diagnostics 2020;10:558.
[12] Ichikawa Y, Kanii Y, Yamazaki A, Nagasawa N, Nagata M, Ishida M, et al. Deep learning image reconstruction for improvement of image quality of abdominal computed tomography: comparison with hybrid iterative reconstruction. Jpn J Radiol 2021;39:598–604.
[13] Akagi M, Nakamura Y, Higaki T, Narita K, Honda Y, Zhou J, et al. Deep learning reconstruction improves image quality of abdominal ultra-high-resolution CT. Eur Radiol 2019;29:6163–71.
[14] Bernard A, Comby PO, Lemogne B, Haioun K, Ricolfi F, Chevallier O, et al. Deep learning reconstruction versus iterative reconstruction for cardiac CT angiography in a stroke imaging protocol: reduced radiation dose and improved image quality. Quant Imaging Med Surg 2021;11:392–401.
[15] Benz DC, Benetos G, Rampidis G, von Felten E, Bakula A, Sustar A, et al. Validation of deep-learning image reconstruction for coronary computed tomography angiography: impact on noise, image quality and diagnostic accuracy. J Cardiovasc Comput Tomogr 2020;14:444–51.
[16] Sakai Y, Hida T, Matsuura Y, Kamitani T, Onizuka Y, Shirasaka T, et al. Impact of a new deep-learning-based reconstruction algorithm on image quality in ultra-high-resolution CT: clinical observational and phantom studies. Br J Radiol 2023;96:20220731.
[17] Hata A, Yanagawa M, Yoshida Y, Miyata T, Kikuchi N, Honda O, et al. The image quality of deep-learning image reconstruction of chest CT images on a mediastinal window setting. Clin Radiol 2021;76:115–23.
[18] Greffier J, Dabli D, Hamard A, Belaouni A, Akessoul P, Frandon J, et al. Effect of a new deep learning image reconstruction algorithm for abdominal computed tomography imaging on image quality and dose reduction compared with two iterative reconstruction algorithms: a phantom study. Quant Imaging Med Surg 2022;12:229–43.
[19] Tatsugami F, Nakaura T, Yanagawa M, Fujita S, Kamagata K, Ito R, et al. Recent advances in artificial intelligence for cardiac CT: enhancing diagnosis and prognosis prediction. Diagn Interv Imaging 2023;104:521–8.
[20] Tacher V, Sifaoui I, Kharrat R, Dacher JN, Chevance V, Gallet R, et al. The use of cardiac computed tomography angiography in the assessment of percutaneous left atrial appendage closure: review and experts recommendations endorsed by the Societe francaise d'imagerie cardiaque et vasculaire diagnostique et interventionnelle. Diagn Interv Imaging 2021;102:586–92.
[21] D'Antonio A, Assante R, Zampella E, Mannarino T, Buongiorno P, Cuocolo A, et al. Myocardial blood flow evaluation with dynamic cadmium-zinc-telluride single-photon emission computed tomography: bright and dark sides. Diagn Interv Imaging 2023;104:323–9.
[22] Si-Mohamed SA, Boccalini S, Lacombe H, Diaw A, Varasteh M, Rodesch PA, et al. Coronary CT angiography with photon-counting CT: first-in-human results. Radiology 2022;303:303–13.

[23] Nagayama Y, Emoto T, Hayashi H, Kidoh M, Oda S, Nakaura T, et al. Coronary stent evaluation by CTA: image quality comparison between super-resolution deep learning reconstruction and other reconstruction algorithms. AJR Am J Roentgenol 2023. doi: 10.2214/AJR.23.29506.
[24] Rotkopf LT, Froelich MF, Riffel P, Ziener CH, Reid C, Schlemmer HP, et al. Influence of heart rate and heart rate variability on the feasibility of ultra-fast, high-pitch coronary photon-counting computed tomography angiography. Int J Cardiovasc Imaging 2023;39:1065–73.
[25] Johnson NP, Kirkeeide RL, Gould KL. Coronary anatomy to predict physiology: fundamental limits. Circ Cardiovasc Imaging 2013;6:817–32.
[26] Otgonbaatar C, Ryu JK, Shin J, Woo JY, Seo JW, Shim H, et al. Improvement in image quality and visibility of coronary arteries, stents, and valve structures on CT angiography by deep learning reconstruction. Korean J Radiol 2022;23:1044–54.
[27] Tatsugami F, Higaki T, Kawashita I, Fukumoto W, Nakamura Y, Matsuura M, et al. Improvement of spatial resolution on coronary CT angiography by using super-resolution deep learning reconstruction. Acad Radiol 2023. doi: 10.1016/j.acra.2022.12.044.
[28] Nagayama Y, Emoto T, Kato Y, Kidoh M, Oda S, Sakabe D, et al. Improving image quality with super-resolution deep-learning-based reconstruction in coronary CT angiography. Eur Radiol 2023. doi: 10.1007/s00330-023-09888-3.
[29] Sato H, Fujimoto S, Tomizawa N, Inage H, Yokota T, Kudo H, et al. Impact of a deep learning-based super-resolution image reconstruction technique on high-contrast computed tomography: a phantom study. Acad Radiol 2023. doi: 10.1016/j.acra.2022.12.040.
[30] Greffier J, Barbotteau Y, Gardavaud F. iQMetrix-CT: new software for task-based image quality assessment of phantom CT images. Diagn Interv Imaging 2022;103:555–62.
[31] Richard S, Husarik DB, Yadava G, Murphy SN, Samei E. Towards task-based assessment of CT performance: system and object MTF across different reconstruction algorithms. Med Phys 2012;39:4115–22.
[32] Samei E, Bakalyar D, Boedeker KL, Brady S, Fan J, Leng S, et al. Performance evaluation of computed tomography systems: summary of AAPM Task Group 233. Med Phys 2019;46:e735–56.
[33] Burgess AE, Li X, Abbey CK. Visual signal detectability with two noise components: anomalous masking effects. J Opt Soc Am A Opt Image Sci Vis 1997;14:2420–42.
[34] Burgess AE, Wagner RF, Jennings RJ, Barlow HB. Efficiency of human visual signal discrimination. Science 1981;214:93–4.
[35] Eckstein M, Bartroff J, Abbey C, Whiting J, Bochud F. Automated computer evaluation and optimization of image compression of x-ray coronary angiograms for signal known exactly detection tasks. Opt Express 2003;11:460–75.
[36] Barat M, Jannot AS, Dohan A, Soyer P. How to report and compare quantitative variables in a radiology article. Diagn Interv Imaging 2022;103:571–3.